Rapid Assembly of Large Scale Transparent Circuit Arrays Using PDMS Nanofilm Shaped Coffee Ring

*Yiwei Li, Weixia Zhang, Jiliang Hu, Yachao Wang, Xiaojun Feng, Wei Du, Ming Guo, and Bi-Feng Liu**

Rapid and precise assembly of functional nanoparticles into well-defined structures in large scale is motivated by broad fields. In this study, large-scale transparent conductive circuit arrays are rapidly self-assembled by simply pipetting a gold nanoparticles suspension onto a PDMS nanofilm patterned substrate with distinct hydrophilic/hydrophobic areas. The solution firstly self-confines into predefined hydrophilic geometries, followed by assembly of nanoparticles into well-defined circuits with 1D patterns by coffee ring effect. Submicrometer height and submicrometer- to micrometer-width circuit arrays with various shapes are precisely generated by varying the PDMS nanofilm patterns. Thousands of circuits with different geometries are self-assembled simultaneously within 1 min. The conductive circuits show good optical transparency up to 95%. After being transferred into PDMS elastomer sheet by encapsulating, the circuits remain highly conductive during bending and stretching. With the advantages of high-throughput, equipment-free, scalability, and precise control, this technique will open an avenue for fabricating large-scale functional materials for applications in electronics, optoelectronics, and healthcare devices.

1. Introduction

Precise fabrication of large-scale conductive networks will potentially facilitate the development of electronics[1–5] and further benefit the manufacture of optoelectronic,[6,7] plasmonic,[8,9] magnetic,[10] and healthcare devices.[11] To achieve this goal, various methods have been developed, such as lithography and assembly.[4,5] Particularly, unlike lithography, which requires tedious sample preparation, assembly of nanomaterials, including molecule recognition assembly,[12–14] magnetic assembly,[15,16] nanotube-template assembly,[17] and electrical assembly,[18,19] provides a cheap and simple way to facilitate circuit fabrication. However, these approaches have low efficiency and less control on final patterns. In addition, the length scale of assembled structures is typically limited to hundreds of nanometers to several micrometers.[20]

Alternatively, assembly of nanoparticles via solvent evaporation has been recognized as an extremely facile and easily scalable route to fabricate structures with less cost,[21–27] although regular evaporation-induced assembly suffers from irregular features such as isolated islands, worm-like domains, ring-like structures, and cellular networks.[22,28,29] The coffee ring effect arising from evaporation draw much attention and has inspired researchers to develop new approaches in nano/microscale fabrication. Several methods have been proposed to control evaporative assembly for depositing materials of interest, including two-substrate configuration (plates,[30–33] cylinders,[34–37] curves,[21,38–44] or polydimethylsiloxane (PDMS) molding[22]), liquid bridge (with inkjet[20] or sandwiched pillars[45]), and confined droplet (with inkjet,[46] chemically patterned surface,[47–53] or protrusions of stamps[54–56]). However, it is still not easy to precisely shape ring structure into arbitrary multifarious functional patterns due to the undesired receding contact lines and fingering instabilities in confined sessile droplets evaporation.[22] Furthermore, specific setups and multiple fabrication steps with complex manipulations are still required.[20] Thus, how to rapidly and simultaneously fabricate a large number of heterogeneous circuits in a simple way is still a challenge, which greatly impedes its wide applications in large-scale electronics manufacture.

In this paper, we develop a one-step method to rapidly fabricate conductive circuit arrays by using PDMS nanofilm shaped coffee ring. The whole procedure is simply pipetting gold nanoparticle (AuNPs) solution onto a PDMS nanofilm patterned substrate without using any sophisticated equipment. The nanoparticles then self-assemble into a network at clear-cut, predefined contact line boundaries by the wettability confinement

Dr. Y. W. Li, Y. C. Wang, Prof. X. J. Feng, Prof. W. Du, Prof. B.-F. Liu
The Key Laboratory for Biomedical Photonics of MOE at Wuhan National Laboratory for Optoelectronics, Hubei Bioinformatics and Molecular Imaging Key Laboratory
Systems Biology Theme
Department of Biomedical Engineering
College of Life Science and Technology
Huazhong University of Science and Technology
Wuhan 430074, China
E-mail: bfliu@mail.hust.edu.cn
Dr. Y. W. Li, J. L. Hu, Prof. M Guo
Department of Mechanical Engineering
Massachusetts Institute of Technology
Cambridge, MA 02139, USA
Dr. W. X. Zhang
John A. Paulson School of Engineering and Applied Sciences
Harvard University, Cambridge
MA 02138, USA

DOI: 10.1002/adfm.201606045

and coffee ring effect. We demonstrate that thousands of heterogeneous circuits with well-controlled dimensions (submicrometer height, submicrometer to micrometer wide, up to one meter long) can be simultaneously self-assembled on a large area (75 mm × 50 mm glass substrate) within 1 min.

2. Results and Discussion

2.1. Overview

A schematic overview of the experiments reported in the paper is shown in **Figure 1**. It shows a substrate with distinguished hydrophilic/hydrophobic patterns by stamping a PDMS nanofilm onto a glass slide (Figure 1a). The conductive circuit arrays were fabricated with the PDMS nanofilm patterned substrate, which automatically produced sessile nanoparticle-encapsulating droplet arrays with predefined shapes and sizes (Video S1, Supporting Information). The nanoparticles inside the sessile droplets self-assembled into the finial circuit arrays with well-aligned 1D wires by the evaporation-induced coffee ring effect (Figure 1b). After being transferred to elastomer substrate, the assembled circuit arrays were applicant to transparent flexible electronics.

2.2. Fabrication and Characterization of PDMS Nanofilm Patterned Substrate with Distinguished Wettability

Practically, we first prepared PDMS nanofilm patterned substrate using a widely accessible PDMS reversible bonding method (Figure 1a, Figure S1, Supporting Information).[57] A PDMS stamp with predefined concave pattern was fabricated using the conventional soft lithography and rapid prototyping. The PDMS stamp and a glass substrate were treated with oxygen plasma and then temporarily bonded together (Figure 1a, Step 1). After bonding, we immediately peeled the PDMS layer off (Figure 1a, Step 2). The bonding areas on the glass were coated with a layer of PDMS nanofilm (Figure 1a, Step 3). The PDMS nanofilms showed a shattered multiple layered structure (**Figure 2**) with a thickness of 100 nm, probed by atomic force microscopy (Figure 2b). The physical boundary of the PDMS nanofilm, which was precisely predesigned as the pinned three-phase contact line (Figure 2a), would be the final position of deposited nanoparticles. The hydrophobic PDMS nanofilm coating layer rendered the underneath hydrophilic glass surface. Thus, the PDMS patterned area showed a hydrophobic property by both changing the surface chemistry (Figure 2d) and increasing the surface nanotopography roughness (Figure 2a,b). The PDMS nanofilm boundary exhibited distinct wettability (Figure 2e) and topography on two sides (Figure 2a,b). The hierarchical nanostructure combining with different surface wettability contributed to the pinned three phase contact line, which helped prevent receding contact lines during sessile droplet evaporation in a well-controlled environment (65 °C and less than 10% humidify). The clear-cut contact line boundary between hydrophilic/hydrophobic areas with combined distinguish physical/chemical property gave our method precise control over droplet shaping and nanomaterials deposition.

2.3. Rapid Assembly of Circuit Arrays Demonstrated by Quantum Dots (QDs)

To generate circuits, we simply pipetted the nanoparticles suspension onto the top of the PDMS nanofilm patterned substrate as shown in Figure 1b. The PDMS nanofilm pattern caused wetting of aqueous solutions to hydrophilic regions (without covered nanofilm) and repulsion of aqueous solutions to hydrophobic regions (with nanofilm). Thus, the microscale small droplets were produced simultaneously as the large droplet moved across the surface of the wettability-patterned substrate via a glass tip, during which nanoparticle-containing

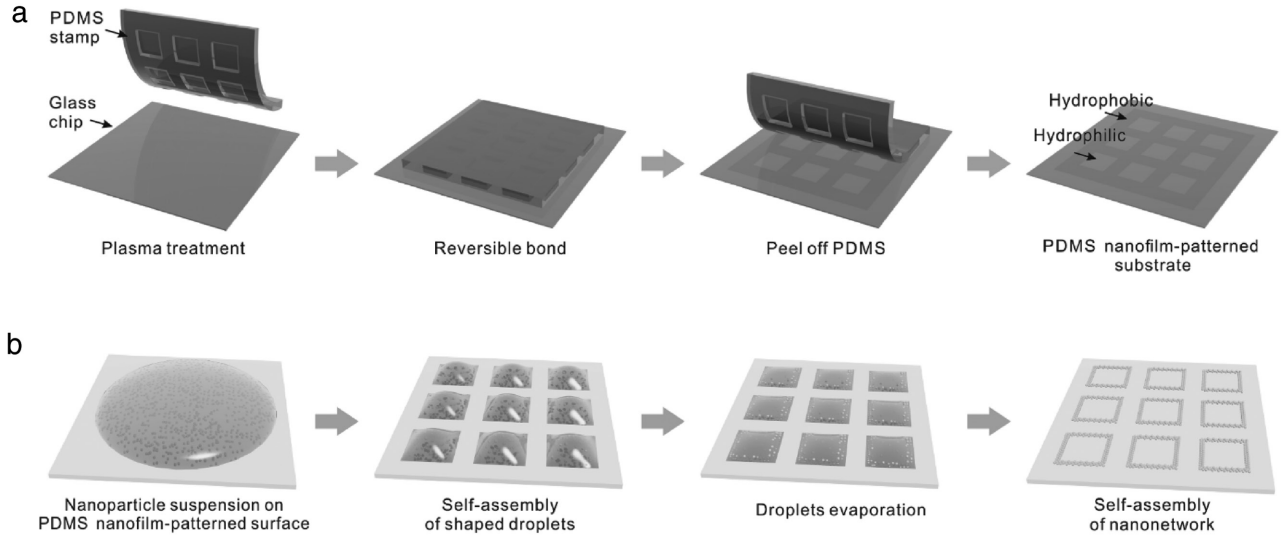

Figure 1. Schematic illustration of assembly of circuit arrays using PDMS nanofilm-shaped coffee ring. a) Schematics of fabrication of PDMS nanofilm patterned substrate. b) Schematics of assembly of circuit arrays guided by wettability-shaped coffee ring.

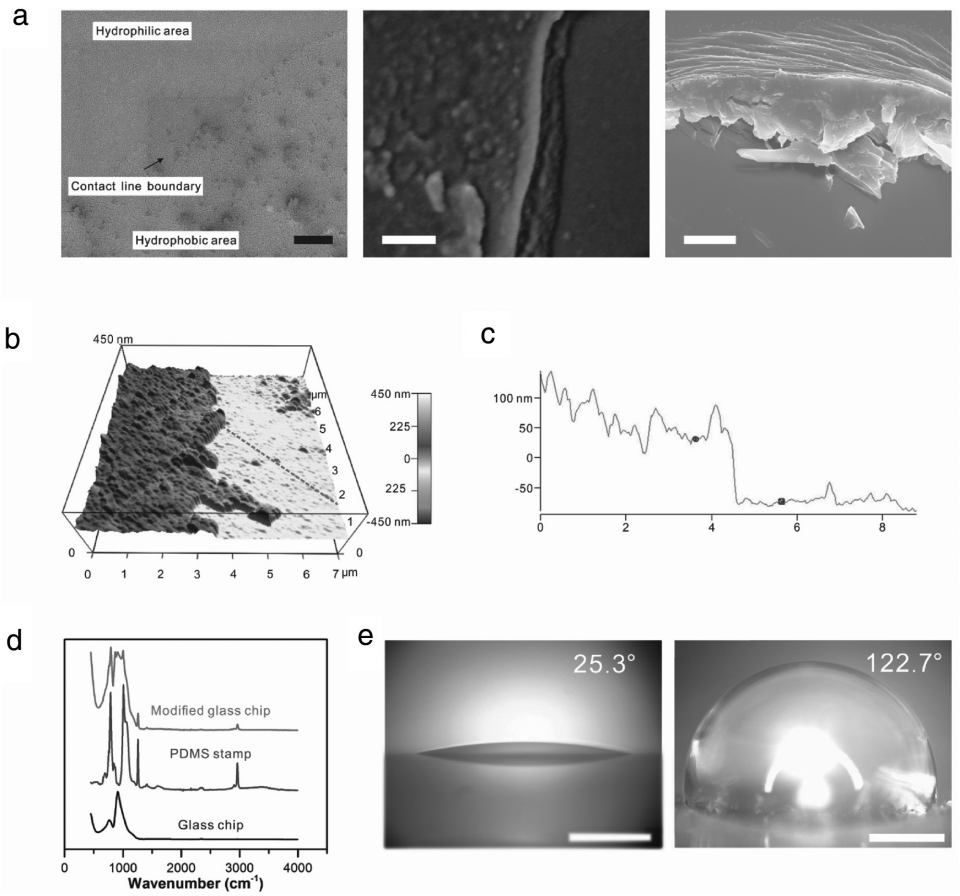

Figure 2. Characterization of PDMS nanofilm patterned substrate. a) SEM images of physical boundaries of the PDMS nanofilm. The nanotopographies on two sides of the contact line boundaries are different. The section image of the nanofilm boundary is showed with 30° tilting view. Scale bar, 2 μm, 200, and 100 nm from left to right. b) AFM image of PDMS nanofilm patterned substrate. c) The line profile probed by AFM as indicated in (b), showing the height of the PDMS nanofilm ranging from 100 to 200 nm. d) ATR-FTIR analysis of PDMS nanofilm patterned substrate. e) Water contact angles on hydrophilic region (without PDMS nanofilm) and hydrophobic region (with PDMS nanofilm) respectively. Scale bar, 500 μm.

droplet array with various geometries assembled within a few seconds (Figure S2, Supporting Information). By measuring the sizes and the total fluorescence of each individual microdroplets in the array, we demonstrated a coefficient of variation less than 3% (Figure S3, Supporting Information). And unlike natural water droplets, which usually have quasi-spherical cap shapes, PDMS nanofilm shaped microdroplets were well-defined with shapes, volumes, locations, and most importantly, physically pinned contact lines. And these shaped microdroplets displayed identified, highly controlled dewetting dynamics. During evaporation, nanoparticles in droplets self-assembled into the predefined triphase contact line boundaries to form the final conductive circuits within 1 min, which was firstly demonstrated for visualization by QDs (**Figure 3**a).

QDs were first used to assemble the polygon to demonstrate this method, which is a new class of materials for light emitting diodes, photovoltaic devices, and biosensors. First, circuit arrays with various geometries were assembled as shown in Figure 3b (triangle, rectangle, circle, cross, square, and octagon). The largest distance in all six kinds of individual circuits was designed to be 600 μm. By measuring the side length of different patterns, we demonstrated a coefficient of variation less than 2% in all varied patterns, confirming that we could precisely control the patterns and sizes of the circuits. By measuring the total fluorescent intensity of each pattern, we showed the variations in the mass of assembled nanomaterial are also below 5% (Figure S4, Supporting Information). For each pattern, an 83 × 55 array with a total scale of 75 mm × 50 mm was self-assembled in 1 min, which indicated that this shaped coffee ring based fabrication could be easily scaled up. A heterogeneous circuit array containing different structures was also demonstrated to show that large numbers of circuits with varied structures could be fabricated simultaneously (Figure S5, Supporting Information). We further demonstrated a large-scale, interconnected, wavy-shaped polygon, which was widely used in flexible and stretchable electronics (Figure 3c). The intervals of wires were around 200 μm, and the total length of each wire is up to 1 m.

2.4. Rapid Assembly of Circuit Arrays Demonstrated by Polystyrene (PS) Nanoparticles

To further demonstrate the versatility of our method, we also tested organic polymer nanoparticles. The monodispersed PS

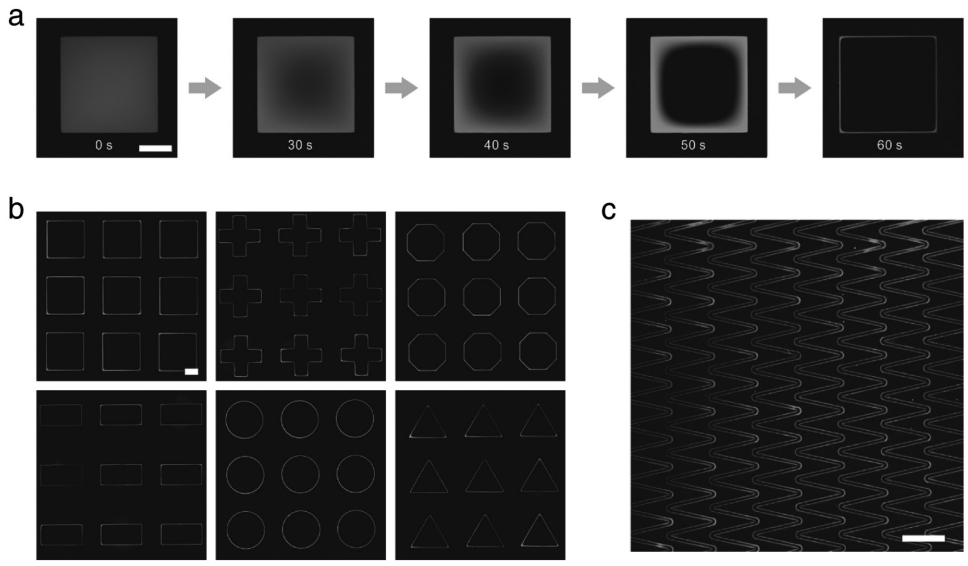

Figure 3. Assembly of circuit arrays demonstrated by quantum dots (QDs). a) Time sequential images of circuits assembled with QDs. Scale bar, 200 µm. b) Self-assembled circuit arrays with various geometries demonstrated with QDs. Scale bar, 200 µm. c) Assembled circuit arrays with wavy geometry demonstrated with QDs. Scale bar, 2 mm.

nanoparticle of a diameter of 100 nm was chosen as a model. The size of the PS nanoparticles was comparable to the thickness of the PDMS nanofilm, which clearly showed the distributions and architectures of the wires. The PS wire showed that the particles were clearly assembled on the edge of the PDMS nanofilm (**Figure 4**a). The images showed almost no particles located in the hydrophobic area and inner hydrophilic area (Figure 4b). As we observed, if we slowed down the evaporation speed by decreasing the temperature, the location where particle deposited slightly recedes. The receding distance, defined as the distance between the assembled nanoparticle line and the edge of the PDMS nanofilm, ranged from 0 to 5 µm as the temperature decreased from 80 to 20 °C. The results can be explained by the slower pinning of the contact line at a lower temperature due to solvent evaporation. With a lower temperature, the decreased rim evaporation suppresses coffee ring formation because a cooler environment retards edge evaporation more than that in the center. On the contrary, a higher temperature enhanced evaporation near the droplet's edge more than that at the center, which

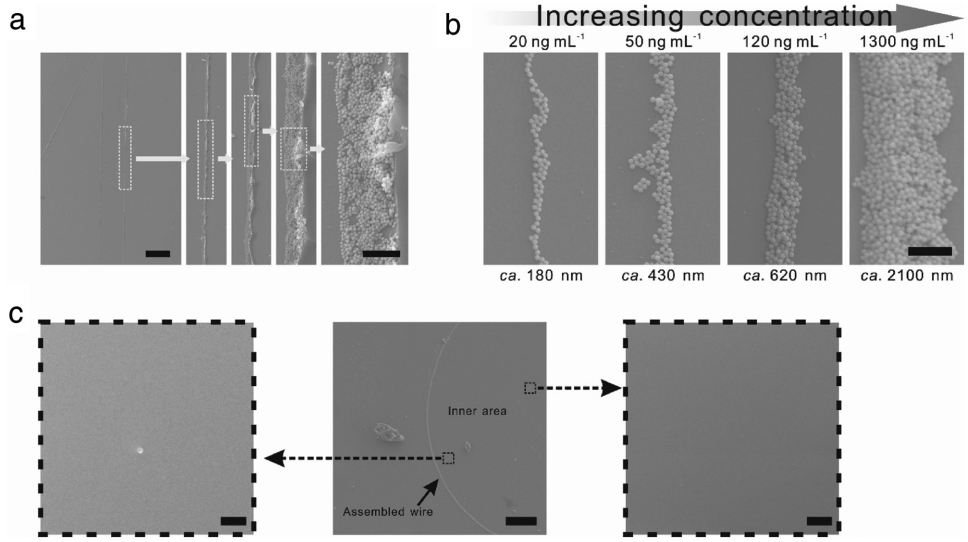

Figure 4. Characterization of assembled wires demonstrated by polystyrene (PS) nanoparticles. a) SEM images of single PS colloid wire of wavy-shaped circuits located on the boundary of hydrophilic/hydrophobic areas. Scale bar, 200 µm (left), 1 µm (right). b) SEM images of PS colloid wires with various widths. Scale bar, 800 nm. c) SEM images showing that no particle deposited on the inner area after assembly. SEM image of assembled circle wire (middle, scale bar, 60 µm). Enlarged SEM images shows that no particle deposited on the center inner area (right, scale bar, 2 µm) and the inner area near the assembled wire (left, scale bar, 2 µm).

increases the amount of nanoparticles transferred toward the three-phase contact line. Assembly in an environment with a temperature higher than 65 °C confirmed that the particles deposited onto the edge of the PDMS nanofilm. If we further increased the temperature higher than 80 °C, the assembly failed due to immediate evaporation of the solvent (Figure S6, Supporting Information). When the temperature was higher than 85 °C, the particles were deposited into an annulus area of the hydrophilic pattern as shown in Figure S6 in the Supporting Information. This annulus pattern was generated by the immediate evaporation of the solution under a high temperature, in which the droplet dried out before all the particles moved to the edge of the PDMS nanofilm. We also observed that the annulus pattern had a larger cover area with a higher temperature, indicating more particles deposited before moving to the edge due to a higher evaporation rate. Thus, the optimized temperature should be 65 to 80 °C. We further showed the PS wires with various widths by increasing the initial concentration of the PS particle suspension (Figure 4c). The smallest width we assembled is ≈180 nm with one to three particles side-by-side packaged in width. If we further decreased the initial concentration of the PS colloid particle, the wire would be broken. Here, by assembling QDs and PS nanoparticles, we demonstrated that the PDMS-shaped coffee ring fabrication provided a universal strategy to pattern and align 1D wires of a wide variety of nanoparticles.

We further tested the assembly of PS particles with various diameters up to 3 µm (Figure S7a, Supporting Information). The assembly worked well for particles with a size smaller than 1 µm. On the contrary, even though we could fabricate ca offee ring pattern from the particles with a diameter of 3 µm, there would be a large portion of particles deposited into the inner area of the pattern. We also tested a mixture suspension containing PS nanoparticles with various sizes of 0.5 and 1 µm (Figure S7b, Supporting Information). We observed that almost all particles of 0.5 µm were deposited to the edge of the coffee ring. Meanwhile, even though most particles with a diameter of 1 µm moved to the edge of the coffee ring, there were still a small portion remaineingin the inner area of the hydrophilic pattern. Conclusively, the particles with larger size would be more easily deposited iono the inner area of the hydrophilic pattern. The reason of the size-dependent deposition should be the competition between the deposition rates and the capillary flow rates. For particle deposition, the thickness of the droplet was decreasing during evaporation, as a result, the particles with larger diameter attached to the bottom substrate easier and earlier than the smaller one. Meanwhile, the moving speed of the particles caused by evaporation decreased as the particle size increasing. Thus, the smaller particles were more likely to be brought to the three-phase contact line by the evaporation i-duced capillary flow.

2.5. Rapid Assembly of Conductive Circuit Arrays by AuNPs

To explore the application toward electronics, conductive circuit arrays were fabricated by self-assembling the AuNPs (Figure S8, Supporting Information). We first assembled AuNPs circuit arrays with various shapes. To access the detailed structure of circuits, scanning electron microscopy (SEM) was used to characterize the nanostructure of the fabricated circuits made of AuNPs. **Figure 5**a showed SEM images of two circuits with circular shape and triangle shape, as well as an enlarged corner of a square-shaped circuit, which confirmed the gold nanoparticles were assembled exactly at the position of the physically defined contact line boundary. Most AuNPs migrated to the three-phase contact line due to the coffee ring effect. Nonuniform evaporation flux of the shaped droplets resulted in capillary fluid flowing to replenish the evaporation loss at the edge, which brought nanoparticles to the edge and depositing at the three-phase contact line, and it is obvious that the nanotopographies on two sides of the deposited wire were different, as indicated in Figure 5a. The enlarged SEM images also showed that the individual wire was assembled from colloidal AuNPs (Figure 5b). As we observed, the width of a single assembled wire ranged from 0.2 to 3 µm as indicated by the SEM image, while the heights of these assembled wires ranged from 36 nm to 0.8 µm, as indicated by AFM height profiles (Figure S9, Supporting Information).

The concentration of the AuNPs solution is critical for our fabrication. By varying the concentrations of the nanoparticle suspension, we could control the width of the assembled wire. To verify this, we assembled circle-shaped circuits using AuNPs suspensions of five different concentrations (0.2, 0.4, 1, 2.7, and 10 mg mL^{-1}). The widths of the wires were measured from the SEM images (Figure 5c), which ranged from 200 nm to more

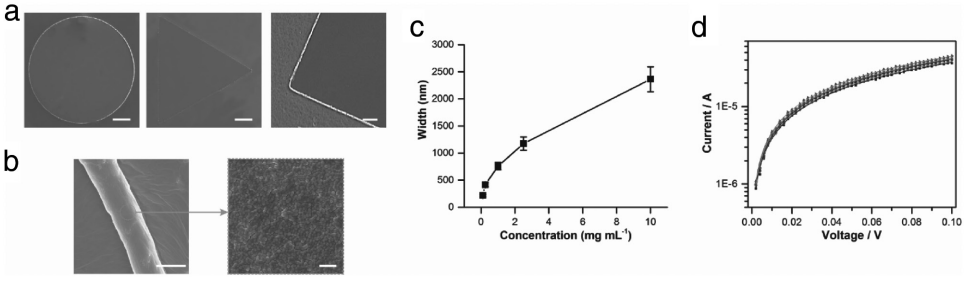

Figure 5. Characterization of conductive circuit arrays assembled by gold nanoparticles (AuNPs). a) SEM images of assembled circle (left) and triangle-shaped (right) circuits. Scale bar, 100 µm. An enlarged SEM image of one corner of assembled square-shaped circuits (right). Scale bar, 5 µm. b) SEM image and enlarged image of individual wire assembled from colloidal AuNPs. Scale bar, 1 µm (left) and 100 nm (right). c) The widths of wires assembled by gold nanoparticle suspensions with various concentrations. d) Measurements of seven parallel wavy-shaped AuNPs circuits showing good conductivity.

than 2.5 μm. For each data, the width was an average of widths measured in six randomly picked positions of the circuits. By SEM imaging and conductive measurement, we found that there were some breakpoints in the assembled wires if the initial concentration of the AuNPs solution was lower than 1 mg mL^{-1}. If we further increased the concentration to higher than 20 mg mL^{-1}, some irregular features were randomly formed during assembly, as shown in Figure S10 in the Supporting Information, which also slightly lowered the transparency. Here, to ensure both good conductivity and transparency performance, 2 mg mL^{-1} AuNPs were used to form circuits array for further applications.

We further assembled a wavy-shaped AuNPs circuit with the same structure and dimension as shown by the QDs in Figure 3c. To further verify that the conductivity of the circuits was reliable and the large circuits were not broken, we measured their conductivities of the parallel AuNPs circuits. Two platinum probes were used to contact two ends of the circuits, and a constant voltage was applied to detect the corresponding current. The conductivities of seven different circuits with the same wavy pattern were measured to confirm unbroken conductive circuits, showing a coefficient of variation of 6.98% (Figure 5d). The resistivity of the assembled AuNPs was calculated to be up to 5.93×10^{-7} Ω m. Thus, the conductivity of the assembled AuNPs exhibited an electrical conductivity up to 4% of that for bulk gold.

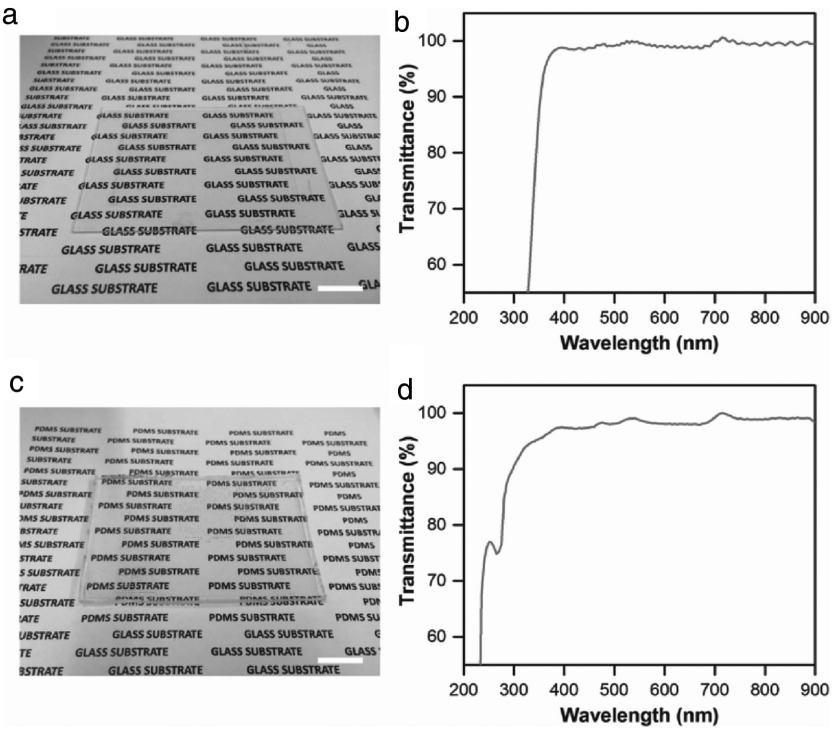

Figure 6. Optical property of assembled gold nanoparticle circuit arrays. a) Optical image of assembled heterogeneous circuit array by wettability-shaped coffee ring on glass substrate. Scale bar, 12.5 mm. b) The transmittance of the assembled circuit arrays on glass substrate. c) Optical image of assembled heterogeneous circuit array by wettability-shaped coffee ring on PDMS substrate. Scale bar, 12.5 mm. d) The transmittance of the assembled circuit arrays on PDMS substrate.

2.6. Good Transparency of the Self-Assembled Circuit Arrays

Transparent conductive circuits are now emerging in a wide range of applications, including displays, lighting devices, solar cells, and more recently, flexible products. In this report, since we can fabricate large-scale circuits with small width and thickness, the glass substrate with assembled circuit arrays exhibited good transparency. To quantify the optical transmittance, a circuits array (83 × 55) of AuNPs with various shapes was fabricated on a 75 mm × 50 mm glass substrate (**Figure 6**a). A UV–vis spectrum was used to measure the transmittance, which was found to be up to 95% from the visible to near infrared region (Figure 6b). Then, we further transferred the conductive circuits from the glass substrate to a PDMS sheet by encapsulation. Briefly, we directly poured the PDMS mixture onto the top of the patterned glass substrate. After curing, the PDMS layer was peeled off the patterned substrate. The conductive circuits were encapsulated inside the PDMS sheet. However, the strong adhesion between the nanoparticles and glass resulted in partially transferring the circuits from glass to PDMS. To achieve complete transfer, we coated a thin film of agarose as a sacrificial layer between the circuits and the hydrophilic substrate (Figure S11, Supporting Information). Briefly, we first fabricated an agarose microgel array on the PDMS nanofilm patterned substrate as we previously reported.[57] 1% low melting point agarose solution was pipetted onto the wettability patterned substrate. The agarose droplet arrays were automatically formed due to the hydrophilic area retaining the liquid while the hydrophobic one repelled the liquid. The formed agarose microgel array was further dried in an oven at 65 °C to complete loss of all the water to form an agarose thin film array, which covered the hydrophilic areas of the PDMS nanofilm patterned substrate. The thin-patterned agarose film showed a smooth surface under the SEM and remained hydrophilic under a humidified environment. Then, the AuNPs circuit arrays were formed as described above. The agarose thin film would be sandwiched between the assembled circuits and the glass substrate, which prevented the strong adhesion between AuNPs and glass. After the circuits' formation, we poured the PDMS monomers onto the top of the circuits array and cured the PDMS polymer at 95 °C, in which the agarose thin film was melted and then released the assembled AuNPs circuits. The released circuits were further encapsulated inside the PDMS sheet after curing (Figure S12, Supporting Information). By employing a sacrificial agarose layer, we achieved the complete transfer from glass to PDMS sheet (demonstrated in Figure S13, Supporting Information).

Another challenging issue was that the hydrophobic area was covered with a PDMS nanofilm, which would be attached

to the PDMS sheet during PDMS mixture curing. To address this problem, we modified the PDMS nanofilm by using perfluorosilane vapor (Figure S14, Supporting Information). Briefly, after the sacrificial agarose layer was fabricated on the wettability-patterned substrate, we placed the wettability-patterned substrate into a sealed container and pipetted a concentrated droplet of perfluorosilane. We ensured that no water was contained and the agarose film was fully dried out before modification. After incubation for several minutes, we rinsed the substrate and assembled the circuits from the nanoparticles. Using this modified substrate, we successfully transferred the circuits to the PDMS sheet. The structure of the circuits and the size of the PDMS sheet were the same as the one with glass substrate used in Figure 3a. As we observed, the PDMS substrate with encapsulated circuits array also showed good transparency (Figure 6c). It was found that transmittance up to 95.2% could be achieved from the visible to near infrared region (Figure 6d).

2.7. Conductivity of the Assembled Circuits during Bending and Stretching

Moreover, such circuits embedded with PDMS sheet were further used as flexible electronics. Circuits with wavy shape were fabricated on PDMS nanofilm patterned substrate and then transferred to the PDMS elastomer sheet. To test the flexibility, the conductivities of the circuits under bending and stretching were tested. **Figure 7**a shows the schematics of the measurement of the electrical test under bending and stretching. For the bending test, three *I–V* curves of different degrees of bending (bending radius r = 2.8, 4 cm) and one *I–V* curve after 100 bending circles are shown in Figure 7b, comparing with the *I–V* curve of the sample without bending. Other samples were tested at different stretching ratios, $(l - l_0)/l$ = 0, 0.06, 0.12. The stretching ratios were obtained by measuring the total length of the PDMS sheet during stretching. The *I–V* curves of different stretching ratios and after 100 stretching circles are shown in Figure 7c. These *I–V* curves demonstrate the good conductivity of the self-assembled circuits during bending and stretching, which potentially benefits the manufacture of flexible devices in multiple areas.

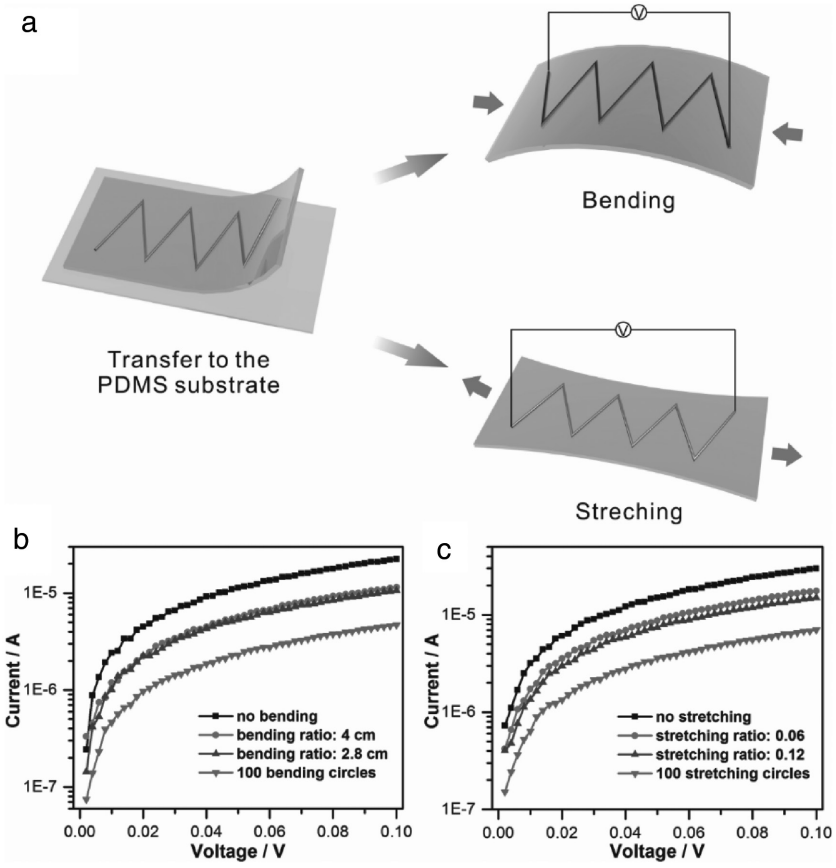

Figure 7. Electrical measurement of wavy-shaped circuit assembled by gold nanoparticle encapsulated in flexible PDMS substrate. a) Schematics of measurements of assembled circuits under bending and stretching conditions. b) *I–V* curves measured between two ends of wavy-shaped circuit under different bending condition: no bending, bending radius 4 cm, bending radius 2.8 cm, and 100 bending circuits, respectively. c) *I–V* curves measured between two ends of wavy-shaped circuit under different stretching condition: no stretching, stretching radius 0.06, stretching radius 0.12, and 100 stretching circuits, respectively.

3. Conclusions

In conclusion, a simple and facile approach to rapidly constructing transparent conductive circuits with minimal operation has been developed based on the PDMS nanofilm shaped coffee ring. Various patterns (triangle, square, circles, rectangle, cross, octagon, and wavy) have been successfully fabricated with a wire of submicrometer height, submicrometer to micrometer width, and up to 1 m long. The scale of the circuits ranges from 0.156 to 3750 mm^2. A heterogeneous circuit array containing 4565 units is rapidly self-assembled in 1 min on the patterned substrate. Our strategy provides spatial control over microdroplet shaping and dewetting. Thus, nanoparticles are assembled exactly at the clear-cut three-phase contact lines, which provide our method with a good precision. This approach is also universally applicable to a wide variety of nanoparticles including QDs and PS nanoparticles. Despite the multiple advantages, such as high-throughput, precise patterning, and easy scale-up, this approach should be further improved to be applicant to industry. Recently, to assemble a certain circuits structure, PDMS nanofilm patterned substrate should be fabricated specifically. The PDMS nanofilm patterned substrates can be fabricated rapidly by simply stamping and peeling as we described, which enables easy scale-up of the manufacture of wettability-patterned substrate. However, practice is still required to achieve good reproducibility, since the operations are currently performed manually. To further improve the throughput and

meet the requirements of industrial manufacture, the automatic machines can be used to replace the manual operations. Overall, this technique might be of use in a broad range of electronic applications, including flexible electronics as well as wearable devices, biomechanical sensing, and healthcare devices.

4. Experimental Section

Fabrication of PDMS Stamp: PDMS stamps were fabricated according to conventional photolithography and rapid prototyping.[58,59] Briefly, a SU-8 master mold with a patterned structure was fabricated on a silicon wafer using standard photolithography. PDMS prepolymer mixture (PDMS precursor and curing agent in a ratio of 10:1) was poured against the SU-8 mold. The PDMS stamp was fabricated after curing at 65 °C for 4 h.

Fabrication of Wettability-Patterned Surface: Glass substrate was prepared simply through rinsing and dehydration. Both glass substrate and PDMS sheet were etched by oxygen plasma using an oxygen plasma machine (420 V, 800 mL min^{-1}, 80 s). Then, the PDMS layer was reversibly bonded to the glass slide. After peeling off the PDMS layer from the glass slide, the authors obtained the wettability-patterned glass substrate.

Measurements of Water Contact Angle: Areas on wettability-pattern glass substrates with or without PDMS nanofilm were prepared for contact angle analysis. Glass substrate should be placed horizontally prior to measurement. Water contact angle measurement was performed by adding a 5 µL water droplet on the surface. A home-built system with commercial digital CMOS camera (Nikon D800) was used to record a side view image of droplet. Quantitative analysis of contact angle was performed using software ImageJ. Each experiment was performed at six different positions to geobtainn average result.

Preparation of AuNPs, QDs, and PS Nanoparticles: Typical AuNPs were synthesized by chemically reducing gold chloride with sodium citrate. AuNPs were finally obtained as a powder after being dried under vacuum at 60 °C. The AuNPs were suspended in water to a certain concentration prior to use. The CdTe QDs functionalized with COOH was purchased from Sigma-Aldrich (USA) with fluorescence λ_{em} of 520 nm.

The monodispersed PS nanoparticles with a diameter of 100 nm were synthesized according to the emulsion polymerization method using sodium lauryl sulfate as emulsifier, potassium persulfate as initiator, and aqueous alcohol (the mixture of distilled water with ethanol) as dispersion medium, respectively. Briefly, the authors dissolved both the potassium persulfate and sodium lauryl sulfate in aqueous alcohol with a 250 mL two-neck flask as a container. Then, the styrene was added under a nitrogen atmosphere and rapid stirring. The emulsion solution was heated to 70 °C for polymerization for 8 h.

The fluorescent-labeled polystyrene latex particles with various diameters of 0.5 and 1 µm were obtained from Sigma-Aldrich (U.S.A.). The fluorescent-labeled polystyrene latex particles with various diameters of 0.2 and 3 µm were obtained from ThermoFisher (USA).

Assembly of Conductive Circuits by Wettability-Shaped Coffee Ring: A large droplet of AuNPs suspension was pipetted onto the top of the glass substrate., ad then the authors carefully wiped the droplet off the substrate using a glass needle. Since the hydrophilic area retained the liquid,while the hydrophobic area repealed the liquid, the AuNPs-contained microdroplet array was generated automatically. After droplet formation, the droplets began to dehydrate via evaporation. During the evaporation, the AuNPs flowed to the triphase pinned line to form the predefined circuits by outward flow induced by unbalance evaporation between droplet edge and center.

Electrical Measurements of the Coffee Ring Circuits: Two platinum contact probes were manipulated to contact two ends of the self-assembled circuits under a conventional inverted microscope (IX71, Olympus, Japan) to measure the resistance with an HP 4156A semiconductor analyzer.

SEM Measurement: SEM images were obtained using ca onventional scanning electron microscope (Philips XL30-FEG) operated at 10 kV. Samples were coated with Pt/Pb by sputtering for 120 s prior to imaging.

Measurement of Transmittance: Assembled circuits on glass substrate or encapsulated in PDMS sheet were prepared respectively for transmittance measurement. All UV–vis transmission spectra were obtained using a commercial UV–vis spectroscopy (Agilent Cary 60). For each sample, spectra at five different positions of the same sample were measured to ensure the results were consistent.

Supporting Information

Supporting Information is available from the Wiley Online Library or from the author.

Acknowledgements

Y.W.L. and W.X.Z. contributed equally to this work. The authors gratefully acknowledge the financial supports from National Natural Science Foundation of China (21475049, 31471257, and 21275060) and National Key R&D Program of China (2016YFF0100801).

Received: November 17, 2016
Revised: December 28, 2016
Published online: February 6, 2017

[1] Y. Cui, C. M. Lieber, *Science* **2001**, *291*, 851.
[2] Z. H. Nie, A. Petukhova, E. Kumacheva, *Nat. Nanotechnol.* **2010**, *5*, 15.
[3] Z. Y. Tang, N. A. Kotov, *Adv. Mater.* **2005**, *17*, 951.
[4] L. Tapasztó, G. Dobrik, P. Lambin, L. P. Biró, *Nat. Nanotechnol.* **2008**, *3*, 397.
[5] W. Lu, C. M. Lieber, *Nat. Mater.* **2007**, *6*, 841.
[6] X. F. Duan, Y. Huang, Y. Cui, J. F. Wang, C. M. Lieber, *Nature* **2001**, *409*, 66.
[7] M. Quinten, A. Leitner, J. R. Krenn, F. R. Aussenegg, *Opt. Lett.* **1998**, *23*, 1331.
[8] D. Solis, B. Willingham, S. L. Nauert, L. S. Slaughter, J. Olson, P. Swanglap, A. Paul, W. S. Chang, S. Link, *Nano Lett.* **2012**, *12*, 1349.
[9] B. Su, Y. C. Wu, Y. Tang, Y. Chen, W. L. Cheng, L. Jiang, *Adv. Mater.* **2013**, *25*, 3968.
[10] S. Singamaneni, V. N. Bliznyuk, C. Binek, E. Y. Tsymbal, *J. Mater. Chem.* **2011**, *21*, 16819.
[11] J. N. Anker, W. P. Hall, O. Lyandres, N. C. Shah, J. Zhao, R. P. Van Duyne, *Nat. Mater.* **2008**, *7*, 442.
[12] M. R. Jones, R. J. Macfarlane, B. Lee, J. A. Zhang, K. L. Young, A. J. Senesi, C. A. Mirkin, *Nat. Mater.* **2010**, *9*, 913.
[13] T. Kodama, A. Jain, K. E. Goodson, *Nano Lett.* **2009**, *9*, 2005.
[14] L. B. Wang, Y. Y. Zhu, L. G. Xu, W. Chen, H. Kuang, L. Q. Liu, A. Agarwal, C. L. Xu, N. A. Kotov, *Angew. Chem., Int. Ed.* **2010**, *49*, 5472.
[15] S. E. Bowles, W. Wu, T. Kowalewski, M. C. Schalnat, R. J. Davis, J. E. Pemberton, I. Shim, B. D. Korth, J. Pyun, *J. Am. Chem. Soc.* **2007**, *129*, 8694.
[16] S. L. Tripp, S. V. Pusztay, A. E. Ribbe, A. Wei, *J. Am. Chem. Soc.* **2002**, *124*, 7914.
[17] G. Hornyak, M. Kroll, R. Pugin, T. Sawitowski, G. Schmid, J. O. Bovin, G. Karsson, H. Hofmeister, S. Hopfe, *Chem. Eur. J.* **1997**, *3*, 1951.

[18] H. Kim, J. Kim, H. J. Yang, J. Suh, T. Kim, B. W. Han, S. Kim, D. S. Kim, P. V. Pikhitsa, M. Choi, *Nat. Nanotechnol.* **2006**, *1*, 117.
[19] A. Rotaru, J. Dugay, R. P. Tan, I. A. Gural'skiy, L. Salmon, P. Demont, J. Carrey, G. Molnar, M. Respaud, A. Bousseksou, *Adv. Mater.* **2013**, *25*, 1745.
[20] S. R. Chen, M. Su, C. Zhang, M. Gao, B. Bao, Q. Yang, B. Su, Y. L. Song, *Adv. Mater.* **2015**, *27*, 3928.
[21] M. Byun, W. Han, F. Qiu, N. B. Bowden, Z. Q. Lin, *Small* **2010**, *6*, 2250.
[22] W. L. Cheng, N. Y. Park, M. T. Walter, M. R. Hartman, D. Luo, *Nat. Nanotechnol.* **2008**, *3*, 682.
[23] W. Han, Z. Q. Lin, *Angew. Chem., Int. Ed.* **2012**, *51*, 1534.
[24] M. Kuang, L. Wang, Y. Song, *Adv. Mater.* **2014**, *26*, 6950.
[25] R. G. Larson, *Angew. Chem., Int. Ed.* **2012**, *51*, 2546.
[26] H. Ma, J. Hao, *Chem. Soc. Rev.* **2011**, *40*, 5457.
[27] H. Ma, R. Dong, J. D. V. Horn, J. Hao, *Chem. Commun.* **2011**, *47*, 2047.
[28] J. X. Huang, R. Fan, S. Connor, P. D. Yang, *Angew. Chem., Int. Ed.* **2007**, *46*, 2414.
[29] C. P. Martin, M. O. Blunt, E. Pauliac-Vaujour, A. Stannard, P. Moriarty, I. Vancea, U. Thiele, *Phys. Rev. Lett.* **2007**, *99*, 1161037.
[30] B. H. Kim, D. O. Shin, S. J. Jeong, C. M. Koo, S. C. Jeon, W. J. Hwang, S. Lee, M. G. Lee, S. O. Kim, *Adv. Mater.* **2008**, *20*, 2303.
[31] H. S. Kim, C. H. Lee, P. K. Sudeep, T. Emrick, A. J. Crosby, *Adv. Mater.* **2010**, *22*, 4600.
[32] B. G. Prevo, O. D. Velev, *Langmuir* **2004**, *20*, 2099.
[33] H. Yabu, M. Shimomura, *Adv. Funct. Mater.* **2005**, *15*, 575.
[34] M. Abkarian, J. Nunes, H. A. Stone, *J. Am. Chem. Soc.* **2004**, *126*, 5978.
[35] Y. Lin, E. Balizan, L. A. Lee, Z. Niu, Q. Wang, *Angew. Chem., Int. Ed.* **2010**, *49*, 868.
[36] Y. Lin, Z. Su, E. Balizan, Z. Niu, Q. Wang, *Langmuir* **2010**, *26*, 12803.
[37] Z. Lin, S. Granick, *J. Am. Chem. Soc.* **2005**, *127*, 2816.
[38] S. W. Hong, J. Xu, Z. Q. Lin, *Nano Lett.* **2006**, *6*, 2949.
[39] S. W. Hong, J. Xia, Z. Lin, *Adv. Mater.* **2007**, *19*, 1413.
[40] J. Xu, J. Xia, Z. Lin, *Angew. Chem., Int. Ed.* **2007**, *46*, 1860.
[41] S. W. Hong, W. Jeong, H. Ko, M. R. Kessler, V. V. Tsukruk, Z. Q. Lin, *Adv. Funct. Mater.* **2008**, *18*, 2114.
[42] S. W. Hong, M. Byun, Z. Lin, *Angew Chem., Int. Ed.* **2009**, *48*, 512.
[43] S. W. Hong, J. Wang, Z. Lin, *Angew. Chem., Int. Ed.* **2009**, *48*, 8356.
[44] M. Byun, N. B. Bowden, Z. Lin, *Nano Lett.* **2010**, *10*, 3111.
[45] B. Su, C. Zhang, S. R. Chen, X. Y. Zhang, L. F. Chen, Y. C. Wu, Y. W. Nie, X. N. Kan, Y. L. Song, L. Jiang, *Adv. Mater.* **2014**, *26*, 2501.
[46] Z. L. Zhang, X. Y. Zhang, Z. Q. Xin, M. M. Deng, Y. Q. Wen, Y. L. Song, *Adv. Mater.* **2013**, *25*, 6714.
[47] A. Kumar, G. M. Whitesides, *Science* **1994**, *263*, 60.
[48] P. Lenz, R. Lipowsky, *Phys. Rev. Lett.* **1998**, *80*, 1920.
[49] H. Gau, S. Herminghaus, P. Lenz, R. Lipowsky, *Science* **1999**, *283*, 46.
[50] P. Lenz, *Adv. Mater.* **1999**, *11*, 1531.
[51] Y. Xia, D. Qin, Y. Yin, *Curr. Opin. Colloid Interface Sci.* **2001**, *6*, 54.
[52] K. H. Lee, S. M. Kim, H. Jeong, G. Y. Jung, *Soft Matter* **2012**, *8*, 465.
[53] E. Ueda, P. A. Levkin, *Adv. Mater.* **2013**, *25*, 1234.
[54] M. Cavallini, F. Biscarini, *Nano Lett.* **2003**, *3*, 1269.
[55] Y. Wu, J. Feng, X. Jiang, Z. Zhang, X. Wang, B. Su, L. Jiang, *Nat. Commun.* **2015**, *6*, 6737.
[56] Y. Wu, J. Feng, B. Su, L. Jiang, *Adv. Mater.* **2016**, *18*, 3063.
[57] Y. Li, P. Chen, Y. Wang, S. Yan, X. Feng, W. Du, S. A. Koehler, U. Demirci, B. F. Liu, *Adv. Mater.* **2016**, *28*, 3543.
[58] Y. Li, X. Feng, Y. Wang, W. Du, P. Chen, C. Liu, B. F. Liu, *Lab Chip* **2015**, *15*, 3203.
[59] Y. Li, D. Chen, Y. Zhang, C. Liu, P. Chen, Y Wang, X. Feng, W. Du, B. F. Liu, *Sens. Actuators, B* **2016**, *225*, 563.